Pulse spreading and correlation loss in shallow water environments with rough sea surfaces and bottoms

Zhi Yong Zhang, David Bartel

Maritime Division, Defence Science & Technology Group
PO Box 1500, Edinburgh, SA 5111, Australia

ABSTRACT

Active sonar pulses suffer time-spreading, distortion, and de-correlation due to multipath propagation and reflections from rough boundaries. Correlation of the received distorted pulse with the transmitted pulse leads to degradation in pulse compression gain in comparison to the ideal case of a received pulse being simply a time-shifted, amplitude-scaled replica propagated along a single direct path. We assess the degradation by first simulating the propagation of linear frequency-modulated (LFM) pulses in shallow water through Fourier synthesis of parabolic equation solutions, and then characterising the time spreading of the pulse envelope after correlation. Rough seafloor interfaces are modelled as random statistical realisations of power-law spectra. Doppler-spreading effects from sea surface motion are ignored, and rough sea surfaces are modelled as frozen statistical realisations of Pierson–Moskowitz spectra. The variation of correlation loss with sound speed profile, sensor depth, pulse bandwidth, and pulse time duration is investigated and discussed in terms of propagation physics. For performance prediction of broadband active sonar, the conventional active sonar equation needs to be revised by including time-spreading or correlation-loss terms, or by modifying the transmission loss term.

1. INTRODUCTION

Broadband pulses and correlation processing are often used by active sonar systems to enhance signal-to-noise ratio and to improve range resolution. A pulse transmitted in an underwater channel propagates to a receiver through different multipaths due to refraction (within the water column) and reflection (from the sea surface and bottom). Different multipaths undergo different time delays and propagation loss. Furthermore, reflections from rough sea surfaces and bottoms also spread and distort the pulses. Therefore the received pulse is spread out in time and distorted in shape. Correlation of the received distorted pulse with a replica of the transmitted pulse leads to a degradation in processing gain in comparison to the ideal case of a received pulse being simply a time-shifted, amplitude-scaled replica propagated from a single direct path. This degradation in processing gain is termed correlation loss.

Based on parabolic equation modelling, previous authors (Miles *et al*., 2003) studied correlation loss in one-way propagation of frequency-modulated signals in shallow water environments with rough sea surfaces. In this paper, we investigate the correlation loss for environments with both rough sea surfaces and rough sea bottoms. The received signal consists of the convolution of the transmitted signal with the impulse response of the channel. The impulse responses are predicted using parabolic equation methods with random realisations of rough sea surfaces and bottoms. The variation of correlation loss with sound speed profile, receiver depth and pulse bandwidth is investigated, compared with earlier work, and discussed in terms of propagation physics.

2. PULSE PROPAGATION AND CORRELATION

2.1 Time Spreading and Correlation Loss

The physics of underwater sound propagation can be interpreted in terms of multipath arrivals with different propagation angles and travel times. For continuous sound transmission, or if the transmitted pulse is sufficiently long, all significant multipath arrivals overlap in time and the usual concept of transmission loss combines all multipaths. However, for short pulse transmissions, not all multipaths will necessarily overlap in time, leading to pulse time spreading or elongation. As a result, there may be a reduction in the intensity around the peak of the received pulse in comparison to the case when all the multipath arrivals overlap. This reduction in intensity is the time spreading loss.

Correlation processing of a received broadband coherent pulse (such as a frequency-modulated pulse) with a replica of the transmitted pulse leads to a correlation function whose envelope has a main lobe with effective duration being approximately the inverse of the signal bandwidth B. This effective duration is generally much shorter than the original pulse length (hence the correlation process is also called pulse compression) and is regarded as the time-resolution of the pulse.

The sound propagation channel can be approximated as a linear filter and the received pulse as a convolution of the transmitted source pulse with the impulse response of the channel. Because convolution and correlation processes are linear and commutable, the order of propagation and correlation processing may be reversed. Therefore the output of the pulse compression processing may be regarded as the time-spread version of the higher-resolution autocorrelation function after propagation. Correlation loss is the time-spreading loss of the autocorrelation function after propagation.

Correlation loss may be regarded as a mismatch loss because the replica correlator is matched to the transmitted pulse, not matched to the received pulse after propagation through the channel with its multipath spreading and other distortion effects. The mismatch means that only a portion of the available energy is processed in generating the peak of the correlation output, which degrades underwater acoustic sensing performance. The usual active sonar equation, written in terms of transmission loss that sums all multipath contributions, needs to be corrected with time spreading or correlation loss terms.

2.2 Different Measures of Correlation Loss

One measure of correlation loss is the ratio of signal energy in the resolution cell E_B over the total energy E in the correlation function (Miles *et al*., 2003)

$$CL = -10\log\left(\frac{E_B}{E}\right), \qquad E_B = \int_{t_0-(\frac{1}{2B})}^{t_0+(\frac{1}{2B})} |r(t)|\, dt\,, \qquad E = \int_{-\infty}^{\infty} |r(t)|\, dt \tag{1}$$

where $r(t)$ is the correlation function, t_0 is the time at which the correlator is at its maximum value, and B is the bandwidth of the replica. The correlation loss thus defined includes not only the effects of channel time spreading but also the effects of energy leakages out of the resolution cell due to correlation processing. That is, there is still a loss even if the received pulse is a perfect replica of the transmitted pulse, due to leakages out of the resolution cell in the auto-correlation function (an example is given later in Fig.1b). In order to represent the correlation loss due to the environment alone, we define a differential correlation loss ΔCL,

$$\Delta CL = CL - CL_0 \tag{2}$$

where CL_0 is the autocorrelation loss from Eq.(1) when $r(t)$ is the autocorrelation function of the transmitted pulse, and CL is the correlation loss from Eq.(1) when $r(t)$ is the correlation function of the received pulse with the transmitted pulse.

Another formula was used in Knudsen (1986) to compute the correlation loss from experimental data which include both signal and noise. The formula is essentially equivalent to using the dB value of the maximum of the normalized correlation.

2.3 Pulse Waveform and Autocorrelation

We use a set of 0.1-s long, linear frequency-modulated pulses at a center frequency of 1500 Hz and swept bandwidth B of 100, 200, 400, 800 Hz. The rise and fall of the pulses are tapered by cosine-squared shading such that the tapered section at each end is 5% of the entire window length. This window is similar to a Tukey (tapered-cosine) window with the taper replaced by a squared cosine. The peak power of each pulse is 220 dB re 1 microPa^2 at 1 m.

Figure 1 shows an example of the transmitted pulse (bandwidth 100 Hz) and its autocorrelation function. The figures give the real part (x) and envelope (z, analytic signal constructed from the Hilbert Transform) of the pulse and its autocorrelation. The real part of the pulse was used as the replica in the correlation processing. The autocorrelation was computed in the time domain. The resolution cell [1/(2B) seconds each side of the peak] is marked by the vertical dashed lines. The autocorrelation loss due to leakage outside the resolution cell for a bandwidth of 100 Hz is CL_0 (B =100 Hz) = 3.744 dB. For bandwidths of 200, 400, and 800 Hz, we found the autocorrelation loss CL_0 is about 0.5 dB greater and stays almost the same beyond 200 Hz, CL_0(B =200 Hz) = 4.324

dB, CL_0(B=400 Hz) = 4.24 dB, CL_0(B = 800 Hz) = 4.25 dB. These autocorrelation losses are used later to compute the differential correlation loss as defined in Eq.(2).

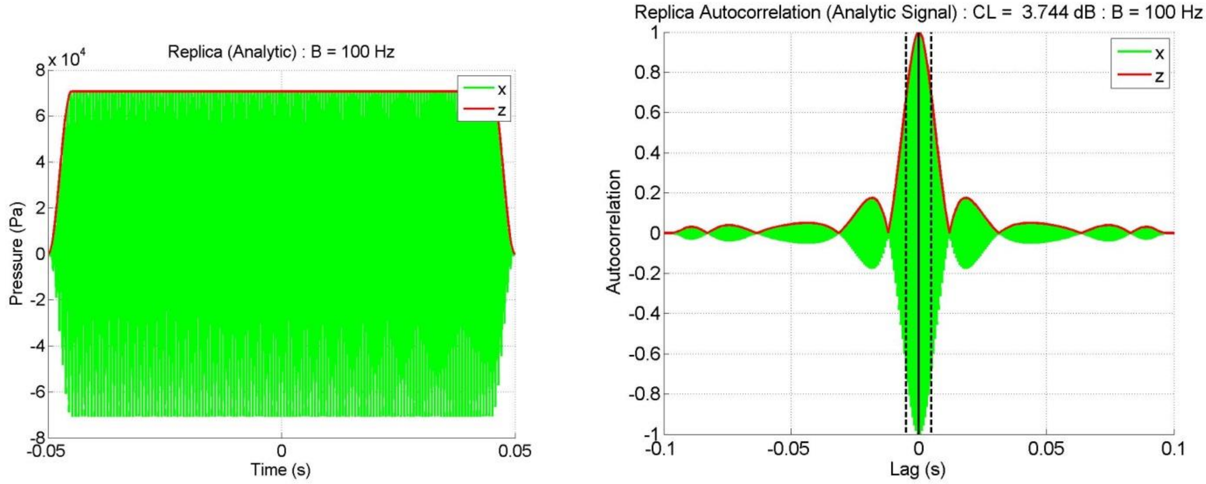

Figure 1: An example of the transmitted pulse (bandwidth 100 Hz) and its autocorrelation function.

2.4 Shallow Water Environments with Rough Boundaries

2.4.1 Sound speed profiles

To compare with previously published work by others, we choose the summer and winter shallow water environments studied in Miles *et al*. (2003:Table II). Both environments have 100 m water depth. The “summer” environment has a weak mixed-layer surface duct of depth 20 m with positive sound speed gradient of 0.015/s, followed by a thermocline with negative sound speed gradient of 0.12/s down to 50 m, and another layer of mixed water with positive sound speed gradient of 0.014/s down to the sediment at 100 m. The “winter” environment has an upward-refracting surface duct of depth 100 m with sound speed gradient of 0.02/s. Both environments have the same sediment parameters that correspond to medium silt. Ray traces for the two sound speed profiles are shown in Fig. 2.

To further investigate the effect of the sound speed profile, we add another environment of isospeed water (1500 m/s) with the same water depth and same sediment.

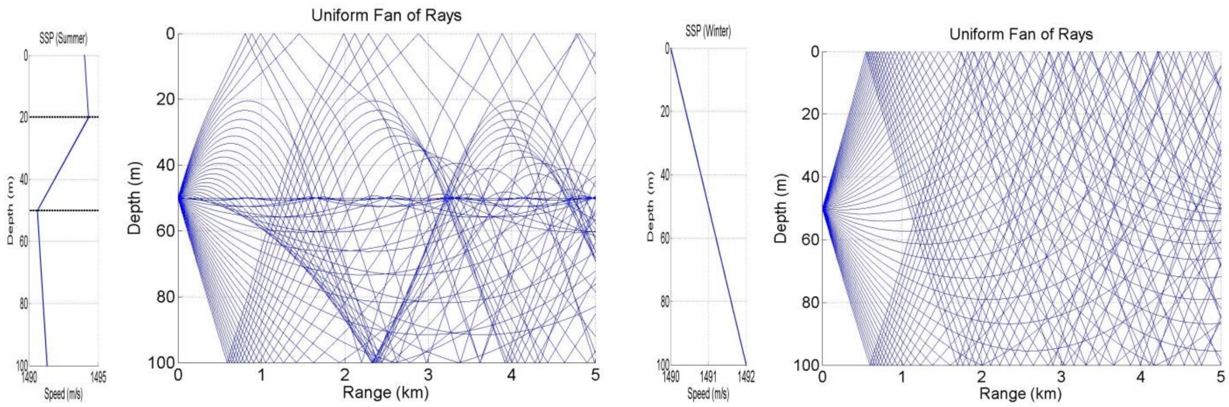

Figure 2: Ray traces for the summer (a) and winter (b) sound speed profiles.

2.4.2 Realisation of rough surfaces and bottoms

Random rough surface and bottom realisations were generated by using the algorithm in equations (17) and (18) of Thorsos (1988) with the appropriate roughness spectra, the Pierson-Moskowitz spectra for fully developed sea surfaces (Pierson-Moskowitz, 1964; Thorsos, 1990) and the power-law spectra for sea floors (Jackson *et al*., 2010: Eq. 5).

For the rough sea-surface realisations, a wind speed of 15 m/s (at 19.5 m above the mean sea surface) was used with the Pierson-Moskowitz spectrum. The evolution of the rough sea surfaces with time, which was implemented in Miles *et al*. (2003) using the water-wave dispersion relation, was ignored and each realisation is independent and uncorrelated from the others.

For the rough seafloor realisations, two roughness spectra of different scales were considered. Spectrum 1 has the “spectral strength” and “spectral exponent” for silt/clay (Jackson *et al*., 2010:Table II) and a “cutoff length” of 100 m. Spectrum 2 has the “spectral strength” and “spectral exponent” for “muddy sandy gravel” (Jackson *et al*., 2010:Table II) and a “cutoff length” of 10 m. The other sediment geoacoustic parameters remain the same as the summer and winter environments in Miles *et al*. (2003), who did not consider rough bottoms.

2.5 Propagation and Correlation Loss

In all the following cases, the transmission loss is computed at a single frequency of 1500 Hz for a point source at a depth of 50 m, using the parabolic-equation model RAM for smooth surfaces (Collins, 1995), RAMSURF for rough surfaces (Folegot, 2013), and an in-house modified version of RAMSURF for rough bottoms. The received pulse time series is generated using Fourier synthesis from complex pressures computed using the RAM or RAMSURF model at sufficiently sampled frequencies within the pulse bandwidth.

2.5.1 Isospeed environment

Figure 3 shows the coherent transmission loss in the isospeed environment with smooth boundaries. At 5 km range there are two high intensity regions around 25 and 75 m depth due to favourable constructive interferences.

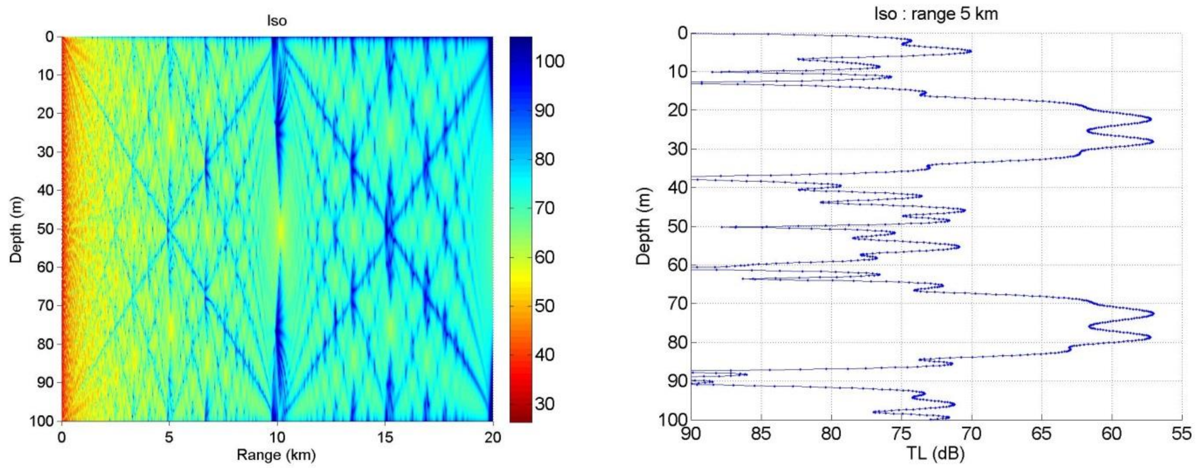

Figure 3: Coherent transmission loss at 1500 Hz for the isospeed environment with smooth boundaries.

Figure 4 shows the pulse time-series and correlation envelopes at 5 km range for the LFM pulses of bandwidths of 100 and 800 Hz transmitted in the same environment. For the narrow bandwidth of 100 Hz, the variation of the pulse intensity with depth closely follows that from transmission at a single centre frequency. As the pulse bandwidth becomes wider at 800 Hz, due to coherent additions of broader-frequency components, the variation of the pulse intensity with depth no longer closely follows that from transmission at a single centre frequency. More multipaths are shown and resolved by the higher-resolution correlation envelopes.

Figure 5a shows the corresponding differential correlation loss at 5 km range for LFM pulses of various bandwidths in the isospeed environment with smooth surfaces. The regions of low loss around 25 m and 75 m depth correspond to the correlation envelopes being more compact with less time spread in Fig. 4. As pulse bandwidth increases, more multipaths are separated in the correlation envelopes and no longer overlap, leading to higher time-spreading/correlation loss.

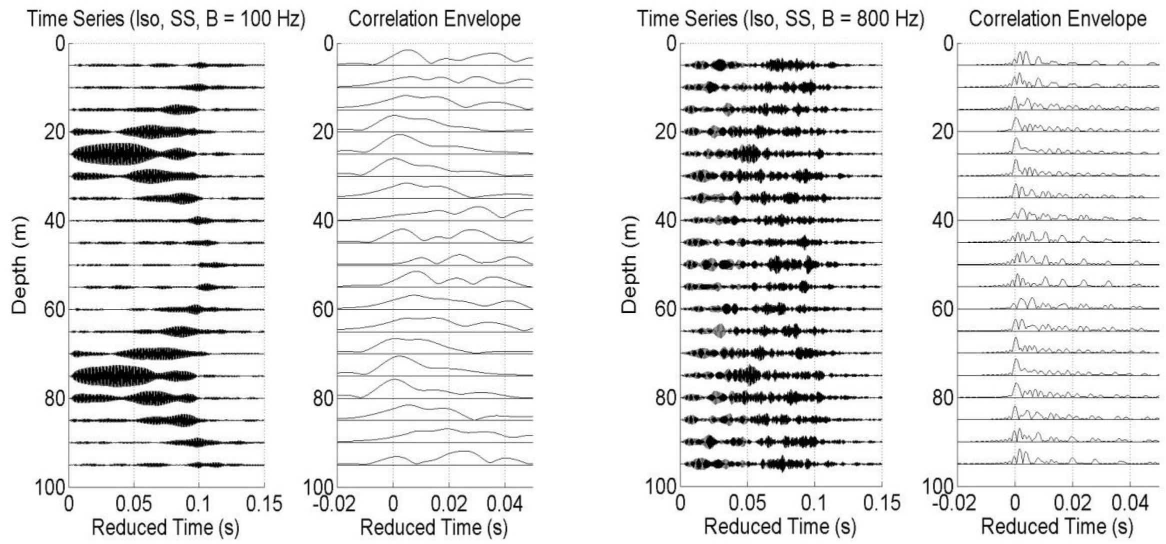

Figure 4: Pulse time series and normalized correlation envelopes at 5 km range and various depths versus reduced time (travel time- range/1500) for LFM pulses of 100 and 800 Hz bandwidth transmitted in the isospeed environment with smooth boundaries.

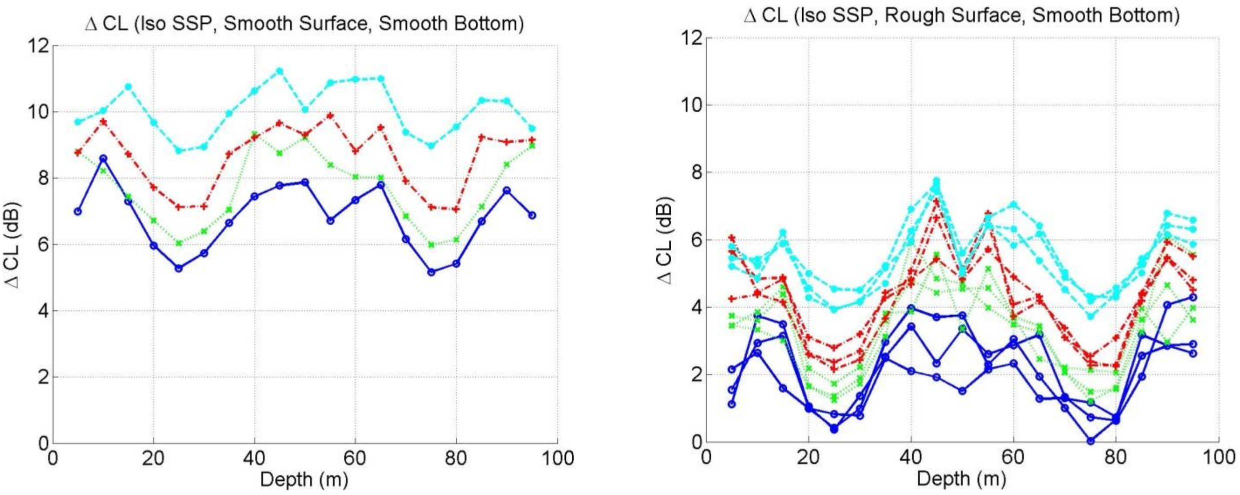

(a) (b)

Figure 5: Differential correlation loss at 5 km range for LFM pulses of various bandwidths (blue:100 Hz; green:200 Hz; red: 400 Hz; cyan: 800 Hz) transmitted in the isospeed environment with smooth (a) and rough (b) surfaces.

Figure 5b shows the differential correlation loss at 5 km range for LFM pulses of various bandwidths in the isospeed environment with three realisations of rough surfaces. The correlation loss follows a similar depth variation as that of the smooth surfaces but is substantially reduced by about 4.5 dB. The reduction in the correlation (time-spreading) loss when the sea surface becomes rough is because the rough surface preferentially removes ("angle stripping") the higher-grazing angle, later multipath arrivals. Rough surfaces scatter more strongly the higher-grazing-angle paths into steeper angles, which suffer greater loss when interacting with the seafloor. Multipaths at shallower angles are scattered less and incur less propagation loss. There is a trade-off between the lower propagation loss and higher time-spreading loss from the flat sea surface and the higher propagation loss and lower time-spreading loss from the rough sea surface.

2.5.2 Summer environment

Figure 6 shows the coherent transmission loss at 1500 Hz in the summer environment with smooth boundaries. The source is on the sound speed minimum and sound ducting occurs at small grazing angles, forming the high intensity regions along the channel axis at 50 m depth. Also, because the negative gradient of the thermocline above the axis is much stronger than the positive gradient below the axis, the sound field below the axis is generally stronger than that above the axis.

Figure 7 shows the pulse time series and correlation envelopes at 5 km range for the LFM pulses of bandwidths of 100 and 800 Hz transmitted in the same environment. Again the variation of the pulse amplitude with depth closely follows that of the transmission at a single centre frequency. And as the bandwidth of the pulses increases, the multipaths become more separated in the higher-resolution correlation envelopes, leading to greater spreading losses.

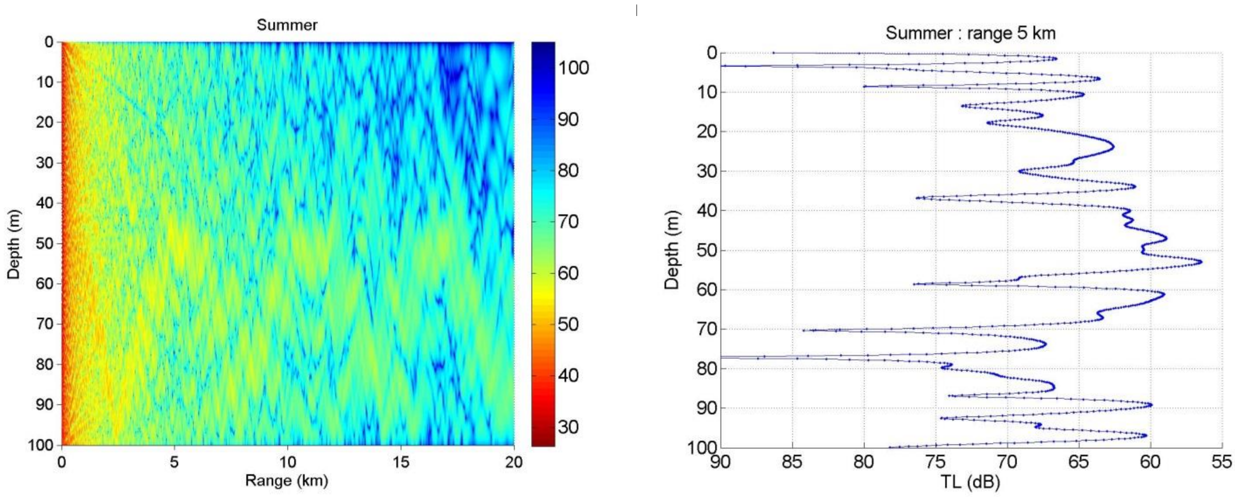

Figure 6: Coherent transmission loss at 1500 Hz for the summer environment with smooth boundaries.

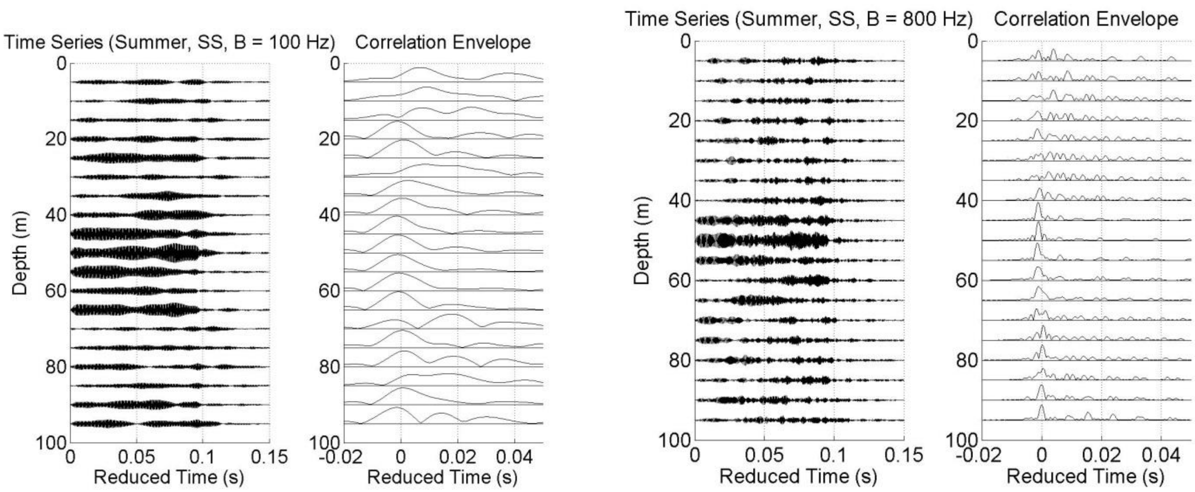

Figure 7: Pulse time-series and normalized correlation envelopes at various depths versus reduced time (travel time- range/1490) at 5 km range for LFM pulses of 100 and 800 Hz bandwidth.

Figure 8a shows the corresponding differential correlation loss at 5 km range for LFM pulses of various bandwidths in the summer environment with a smooth surface and smooth bottom. The correlation loss around 50 m depth is only 1 to 2 dB higher than the autocorrelation loss, indicating the dominance of one (or several closely spaced) ducted propagation path near the channel axis, which is also shown by the high pulse intensities and compact correlation envelopes in Fig.7. As pulse bandwidth increases, the correlation loss also increases, as the multipaths become more separated.

Figure 8b is similar to Fig.8a except the smooth sea surface is replaced by four independent realisations of the rough surface. In comparison to the smooth sea surface, the rough surface increased the correlation loss for shallow (<= 10 m) receivers and slightly reduced the correlation loss for deeper (>15 m) receivers by about 1 dB. The differential correlation loss for the bandwidth of 100 Hz in Fig. 8, after being added to the autocorrelation loss, are consistent with the modelled correlation loss in Miles *et al*. (2003:Fig. 18), which considered LFM pulses of 100 Hz bandwidth only at three receiver depths of 10, 35, 75 m. Around 50 m depth the loss is close to that from the autocorrelation functions, indicating the presence of one dominant propagation path (the slightly negative values for the 100 Hz bandwidth pulse is due to statistical fluctuations). The reduction of the correlation loss due to the rough sea surface is much less than that in an isospeed environment, because the dominant propagation paths for deep receivers do not interact with the rough surface.

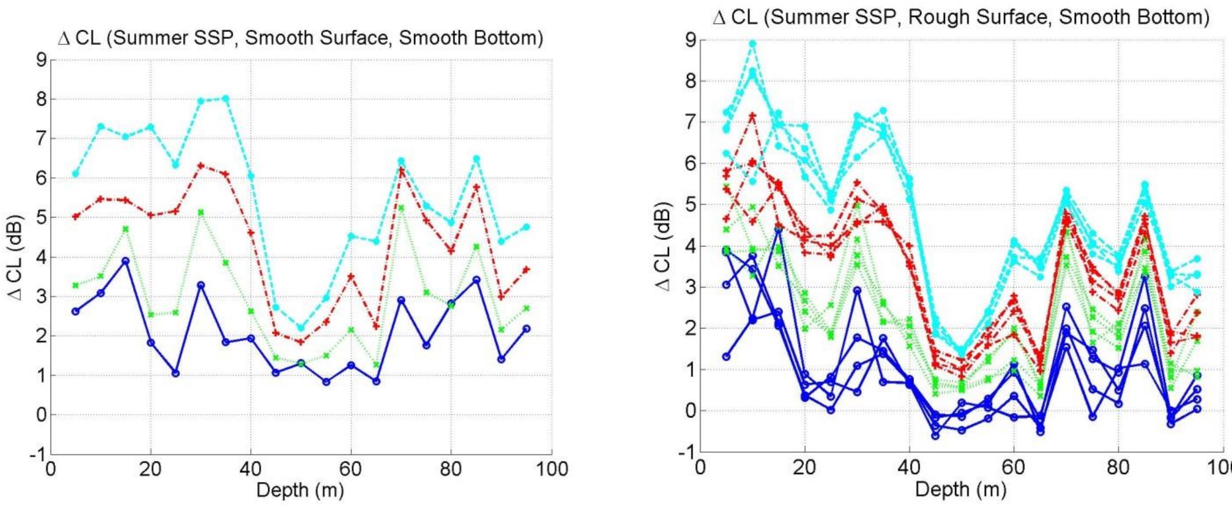

(a) (b)

Figure 8: Differential correlation loss at 5 km range for LFM pulses of various bandwidths (blue:100 Hz; green:200 Hz; red: 400 Hz; cyan: 800 Hz) transmitted in the summer environment with smooth (a) and rough (b) surfaces.

2.5.3 Winter environment

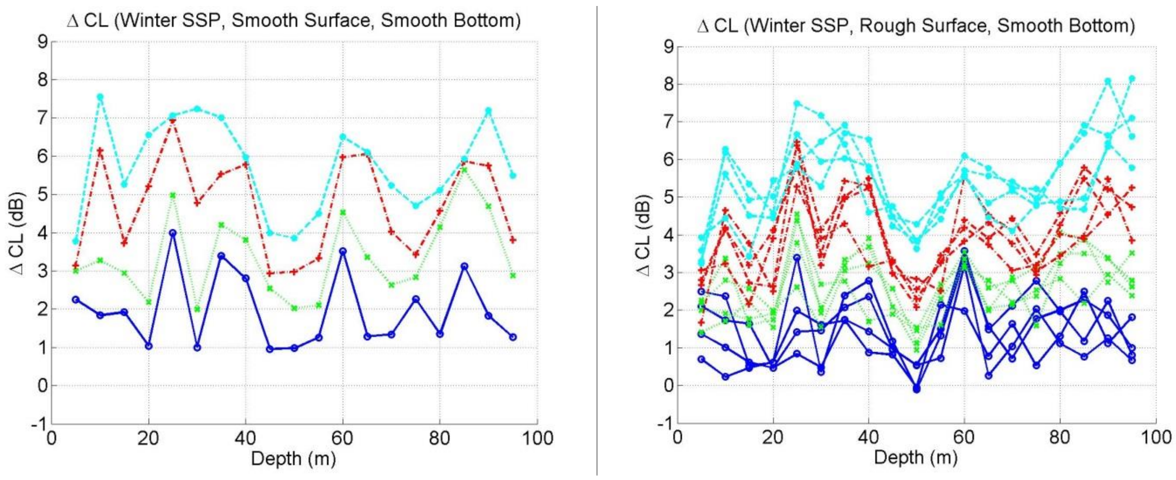

(a) (b)

Figure 9: Differential correlation loss at 5 km range for LFM pulses of various bandwidths (blue:100 Hz; green:200 Hz; red: 400 Hz; cyan: 800 Hz) transmitted in the winter environment with smooth (a) and rough (b) surfaces.

Figure 9a shows the differential correlation loss at 5 km range for LFM pulses of various bandwidths in the winter environment with a smooth surface and smooth bottoms. Figure 9b shows the results when the smooth surface is replaced by four independent rough realisations. These results show a region of small loss around 50 m – the source depth in both cases. The correlation loss increases with increasing pulse bandwidth. The effect of the rough surfaces in reducing correlation loss appears to be small (< 0.5 dB). The differential correlation loss for the bandwidth of 100 Hz in Fig. 8, after being added to the correlation loss of the autocorrelation function, are consistent with the modelled correlation loss in Miles *et al*. (2003:Fig.19), which considered LFM pulses of 100 Hz bandwidth only at three receiver depths of 10, 35, 75 m.

3. DEPTH-AVERAGED CORRELATION LOSS

We arithmetically average the differential correlation loss (before taking the logarithm) across the 19 receiver depths at 5 km range and investigate their variation with sound speed profile, rough surface and bottom, and pulse bandwidth.

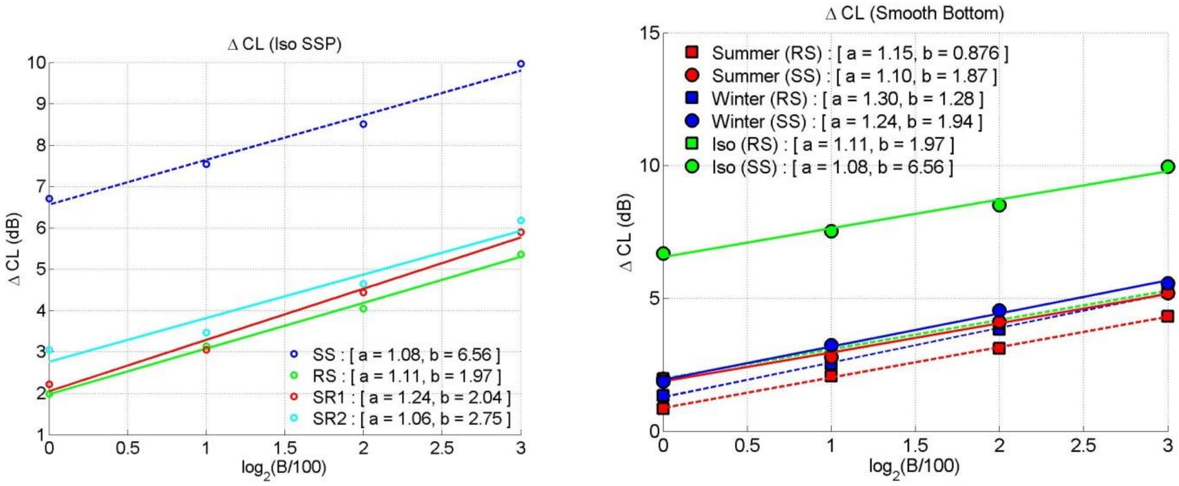

(b) (b)

Figure 10: Depth-averaged differential correlation loss at 5 km range versus bandwidth B of the LFM pulses (see the text for detailed explanations of the meaning of the symbols and parameters).

Figure 10a shows the depth-averaged differential correlation loss at 5 km range for LFM pulses of increasing bandwidths in the isospeed environment with different surfaces and bottoms: "SS" is for smooth surface and smooth bottom, "RS" is for rough surface and smooth bottom, "SR1" and "SR2" are for smooth surface and rough bottom with roughness spectra 1 and 2 respectively, as discussed in section 2.4.2. Figure 10b shows the variation of the depth-averaged differential correlation loss with different sound speed profiles and boundary roughness. The parameters *a* and *b* are linear fits to the following equation,

$$\Delta CL = a \log_2 \left(\frac{B}{100} \right) + b, \quad (3)$$

where *a* is the increase of correlation loss in dB per octave, and *b* is the loss when bandwidth B equals 100 Hz.

3.1 Variation with rough boundaries

Figure 10a shows that in the isospeed environment the typical roughness of seafloor sediments we considered has a comparable effect on reducing correlation loss as the rough sea surface induced by the 15 m/s wind. Figure 10b shows that the rough sea surface has a much stronger effect in reducing correlation loss in the isospeed environment than in the ducted summer and winter environments. This is possibly due to the coupling effects of energy being scattered by the rough sea surface into steeper propagation angles, and the seafloor preferentially absorbing energy at steeper angles. In the isospeed environment, the multipaths interact more strongly with the seafloor than in the summer and winter environments.

3.2 Variation with pulse bandwidth

Figure 10 shows that there is a consistent trend in all the cases where the depth-averaged differential correlation loss increases with increasing pulse bandwidth at between 1.1 and 1.3 dB per octave or between 3.5 and 4.3 dB per decade (to convert to loss per decade, multiply the parameter *a* by $\log_2 10$).

3.3 Variation with pulse duration

We found that increasing the pulse duration from 0.1 s to 0.2, 0.4, 0.8, 1.6, 3.2 s makes negligible difference to the correlation loss, consistent with the experimental findings in Knudsen (1986) for LFM pulse transmissions, albeit in a range-dependent environment with a different sound speed profile. This finding is as expected, since the resolution of the correlation envelope depends not on the pulse duration but on the pulse bandwidth.

4. CONCLUDING REMARKS

We investigated the variation of correlation loss with receiver depth, pulse bandwidth, and different rough surface and bottom conditions for three types of shallow water environments with different sound speed profiles. The results are discussed in terms of propagation physics and are consistent with other published work where available. The correlation loss shows strong dependence on sound speed profile, receiver depth and rough-boundary condition, and increases with pulse bandwidth at about 4 dB per decade. For performance prediction of broadband active sonars, it is suggested that the conventional active sonar equation [e.g., section 9.5 of Waite (2002)] be modified to account for the differential correlation losses. This can be achieved by subtracting the differential correlation losses from the ideal matched filtering gain of a perfect scaled replica, as in Eq.(11.128) of Ainslie (2010), where the term “coherence loss” is equivalent to our differential correlation loss.

A limitation of the present study in using Fourier synthesis methods for pulse propagation in lossy media is the lack of consideration of causality of the resulting propagating pulse. The sound speed must change with frequency (dispersion) in an attenuating medium through the Kramers–Kronig relations (Aki & Richards, 2002; Kulkarni *et al*., 1998) to ensure causality. Real sediments are both dispersive and attenuating (Zhou *et al*., 2009). We neglected the sound speed dispersion in sediments, for simplicity. The error due to this simplification has not been investigated, but is expected to increase with pulse bandwidth. In-water absorption-induced sound speed dispersion is very small near 1500 Hz and was not modelled by us.

Future work may include the investigation of correlation loss of two-way propagated echo pulses, other types of pulse waveforms, downward-refracting sound speed profiles, sound speed dispersion in sediments, comparison with experimental results (Mozzone and Bongi, 1999, Pasewark and Al-Kurd, 1998) and the reduction of correlation loss by using better-matched replicas that account for the pulse distortion induced by the propagation channel.

REFERENCES

Ainslie, MA 2010, *Principles of Sonar Performance Modeling*, Springer-Praxis.

Aki, K. and Richards, P.G., 2002. *Quantitative Seismology*, 2nd Ed.,University Science Books.

Collins, M.D., 1995. User’s Guide for RAM Versions 1.0 and 1.0 p. *Naval Research Lab, Washington, DC*, *20375*.

Folegot T 2013, RAMSurf: RAM recoded in C and vectorized for speed. [updated September 3, 2013]; Available from Ocean Acoustics Library: http://oalib.hlsresearch.com/PE/ramsurf/.

Jackson, D.R., Odom, R.I., Boyd, M.L. and Ivakin, A.N., 2010. A geoacoustic bottom interaction model (GABIM). *IEEE Journal of Oceanic Engineering*, *35*(3), pp.603-617.

Knudsen, T. 1986. “*Measurements of Correlation Loss and Time-Spreading in Linear FM Sweeps and Pseudo-Random Noise Signals Transmitted over Long Ranges in Shallow Water*”, SACLANT ASW Research Centre SM-191, (available from http://stinet.dtic.mil).

Kulkarni, R.S., Siegmann, W.L., Collins, M.D. and McDonald, B.E., 1998. Nonlinear pulse propagation in shallow-water environments with attenuating and dispersive sediments. *The Journal of the Acoustical Society of America*, 104(3), pp.1356-1362.

Miles, D.A., Hewitt, R.N., Donnelly, M.K. and Clarke, T., 2003. Forward scattering of pulses from a rough sea surface by Fourier synthesis of parabolic equation solutions. *The Journal of the Acoustical Society of America*, 114(3), pp.1266-1280. & “Erratum: Forward scattering of pulses from a rough sea surface by Fourier synthesis of parabolic equation solutions" [J. Acoust. Soc. Am. 114, 1266–1280 (2003)]”, *J. Acoust. Soc. Am.* **115**, 1844 (2004).

Mozzone L and Bongi, S, 1999. “Deployable Underwater Surveillance Systems - Analysis of Experimental Results. Part 3”, SACLANT Undersea Research Centre Report, SR-288, April, 1999. (available from http://stinet.dtic.mil).

Pasewark, B. and Al-Kurd, A., 1998. *Acoustic Transmission Loss and Pulse Time-Spread Measured Off the South Carolina Coast During the 1997 Littoral Warfare Advanced Development System Concept Validation Experiment* (No. NRL/MR/7120--98-8138). NAVAL RESEARCH LAB WASHINGTON DC.

Pierson, W.J. and Moskowitz, L., 1964. A proposed spectral form for fully developed wind seas based on the similarity theory of SA Kitaigorodskii. *Journal of Geophysical Research*, *69*(24), pp.5181-5190.

Thorsos, E.I., 1988. The validity of the Kirchhoff approximation for rough surface scattering using a Gaussian roughness spectrum. *The Journal of the Acoustical Society of America*, *83*(1), pp.78-92.

Thorsos, E.I., 1990. Acoustic scattering from a ‘‘Pierson–Moskowitz’’sea surface. *The Journal of the Acoustical Society of America*, *88*(1), pp.335-349.

Waite, A. D. 2002, *SONAR for Practising Engineers*, John Wiley & Sons Inc, 3rd Edition.

Zhou, J.X., Zhang, X.Z. and Knobles, D.P., 2009. Low-frequency geoacoustic model for the effective properties of sandy seabottoms. *The Journal of the Acoustical Society of America*, *125*(5), pp.2847-2866.